Post-print of: Kondratowicz I., Żelechowska K., Nadolska M., Jażdżewska A., Gazda M.: Comprehensive study on graphene hydrogels and aerogels synthesis and their ability of gold nanoparticles adsorption. COLLOIDS AND SURFACES A-PHYSICOCHEMICAL AND ENGINEERING ASPECTS. Vol. 528, (2017), p. 65-73. DOI: 10.1016/j.colsurfa.2017.05.063

Comprehensive study on graphene hydrogels and aerogels synthesis and their ability of gold nanoparticles adsorption

Izabela Kondratowicz[a], Kamila Żelechowska[a] , Małgorzata Nadolska[a], Agata Jażdżewska[b], Maria Gazda[a]

[a] Faculty of Applied Physics and Mathematics, Gdansk University of Technology, Narutowicza 11/12, 80-233, Gdansk, Poland
[b] Faculty of Chemistry, Gdansk University of Technology, Narutowicza 11/12, 80-233, Gdansk, Poland

A B S T R A C T

Graphene hydrogels were prepared by ascorbic acid-assisted gelation of graphene oxide (GO) aqueous suspensions both in acidic and basic conditions. Different mass ratio of ascorbic acid (AA) to GO was used (namely 20:1 and 10:1). In order to eliminate the influence of AA on the final structure of hydrogels, samples without AA were prepared by a hydrothermal gelation of GO in an autoclave. An in-depth structural characterization of the obtained materials was performed before and after supercritical drying by means of FTIR, XRD and SEM. Surface area of hydrogels was determined using the methylene blue adsorption method. BET surface area and pore volume analysis of aerogels was also performed. The effect of initial GO concentration and volume on the final graphene aerogels structure was determined. Electrochemical properties of samples were also evaluated. Finally, gold nanoparticles (Au NP) adsorption on graphene hydro- and aerogels was presented for the first time. Graphene hydrogels and aerogels are promising candidates for practical applications e.g. in the Au NP removal from wastewater.

Keywords: Adsorption, Gold nanoparticles, Graphene aerogel, Graphene hydrogel, Graphene oxide

1. Introduction

To keep up with the pace of technological change, there is a constant need for new materials with improved properties. Among others, carbonaceous nanomaterials are of high interest. CVD graphene foams [1,2], graphene oxide and reduced graphene oxide hydrogels/aerogels [3–5], carbon nanotubes [6–8] or carbonaceous composites [9–12] are promising as alternatives for traditional carbon materials (e.g. glassy carbons, activated carbons). Many recent researches have been focused on the synthesis of three-dimensional porous graphene hydrogels and aerogels using graphene oxide (GO) as a precursor. Such materials have been obtained by a simple and cost-effective hydrothermal treatment of GO aqueous suspension [13–16], or alternatively, by chemically-assisted gelation of GO using ascorbic acid [17–19]. In the hydrothermal method, an autoclave is used and GO suspension is reduced at high temperature and pressure without the addition of reducing agents whereas ascorbic acid-assisted GO reduction can be held at lower temperature and pressure. Different synthesis conditions can be applied in these methods including initial concentration of GO dispersion, GO dispersion volume, reaction temperature and time. Therefore, materials with different properties are expected to be obtained [13–19].

By analysing the results obtained by different scientific groups it can be concluded, that the hydrogel properties strongly depend on the synthesis protocol. For example the reported density was from several mg per cm^3 to nearly hundred mg per cm^3, differences between BET surface areas reached hundreds m^2 per gram [13–19]. Such disparate results clearly shows, that the hydrogel formation is very sensitive to the synthesis parameters, such as GO concentration, volume, pH and presence of the reducing agent.

Although, there are some papers showing the influence of different concentration of GO suspensions [14,15] and the initial pH on the hydrogel properties [16], there are some difficulties with comparing these results as GO from different source and vessels of different shape and volume were used. In this work, we thoroughly studied the properties of graphene hydrogels (GH) and graphene aerogels (GA) synthesized by three different synthesis strategies both in acidic and basic environment. Different concentrations and volumes of GO aqueous suspensions were chosen to study the effect of synthesis parameters on the final graphene structure. Samples were compared in terms of their size, weight, bulk density and water content. Additionally, specific surface areas of hydro- and aerogels were determined by methylene blue (MB) adsorption and BET methods, respectively. Samples were characterized by scanning electron microscopy, X-ray

http://dx.doi.org/10.1016/j.colsurfa.2017.05.063

diffraction spectroscopy and infrared spectroscopy. Electrochemical measurements were also performed to investigate the influence of initial conditions on the electrical properties of hydrogels.

Carbon-based materials have been widely used as adsorbents over the past decades [20–22]. Adsorption is one of the main strategies to purify water because of its ease of operation and low cost. Although the adsorption of many particles and compounds from water (such as heavy metals ions [23–25], metal ions such as Cu(II), Ni(II) etc. [26–28], radionuclides [29], dyes [30–32]) on different carbonaceous materials has already been investigated, the adsorption of metallic nanoparticles (such as gold or silver) on such structures is still not well-studied. A large-scale use of nanoparticles (NP) in modern technologies has recently resulted in their undesired presence in the environment [33–35]. Especially, the recent enhanced usage of Au and Ag nanoparticles in medicine, cosmetics and textiles raises safety concerns due to their release into water, thus appropriate methods of their removal are of high demand. To remove Ag and Au nanoparticles from wastewater some methods are already proposed in the literature including the coagulation [36], flocculation/sedimentation [37] of particles directly from water or the use of functionalized cellulosic paper [38]. There is still no reported data on the Au adsorption on porous graphene-based hydro- and aerogels. High surface area of porous graphene hydrogels endorses their usage as adsorbent. Here, we propose the usage of graphene hydrogel as adsorbent for gold nanoparticles, which served as model nanoparticles. The optical properties of gold nanoparticle solution are related to the concentration of nanoparticles in suspension and therefore the adsorption of Au nanoparticles on graphene materials can be easily quantified by UV–vis spectrophotometry. To the best of our knowledge, there is no comprehensive, systematic studies optimizing graphene hydrogel synthesis with regards to different synthesis parameters and methods. Moreover, the studies on gold nanoparticles adsorption on such graphene hydro- and aerogel structure are still lacking and were performed herein for the first time.

2. Experimental part

2.1. Materials and methods

Graphite flakes, chloroauric acid ($HAuCl_4{\cdot}xH_2O$) were purchased in Sigma-Aldrich. Potassium permanganate ($KMnO_4$), L-ascorbic acid, citric acid, 98% sulfuric acid (H_2SO_4), 85% phosphoric acid (H_3PO_4), 30% hydrogen peroxide (H_2O_2), 35% hydrochloric acid (HCl), 25% ammonia (NH_4OH) and ethanol were purchased in POCh (Gliwice, Poland).

Scanning electron microscopy (SEM) images were obtained using a ESEM Quanta Feg 250, FEI. Fourier transform infrared (FTIR) spectra were performed using Frontier FTIR/FIR PerkinElmer. Samples were prepared in KBr pellets (3%) and were recorded in the range of 4000–400 cm^{-1}. Nitrogen adsorption isotherms was recorded by using Gemini V Micrometrics pore and surface analyser (Micrometrics Instrument Corporation, U.S.A) in the relative pressure range (p/p_0) 0.05–0.9. Before measurement, samples were degassed in N_2 at 200 °C for 2 h. The adsorption analysis was performed at 77 K. Specific surface area results were obtained based on BET method in the relative pressure range (p/p_0) 0.05–0.3. The total pore volume was determined via Barret-Joyner-Halenda (BJH) method. XRD measurements were performed on graphene aerogels using Philips X'PERT PLUS diffractometer with Cu-Kα radiation (λ = 0.154 nm). Magnetic stirrer Heidolph MR hei-standard with hot plate was used and the centrifugation was done using Chemland model P3032 centrifuge with the speed 15000 rpm. UV–vis spectrophotometry (Lambda 10, Perkin Elmer, with a 1 cm quartz cuvette) was used for methylene blue adsorption method as well as for Au nanoparticles adsorption on graphene hydro- and aerogels at a wavelength λ = 664 nm and λ = 530 nm, respectively.

The electrochemical experiments were performed at room temperature, using Ag/AgCl and Pt-mesh as reference and auxiliary electrodes, respectively. The electrochemical measurements were performed using a Reference 600, Gamry Potentiostat/Galvanostat/ZRA supplied by M/S Gamry Instruments (USA). Before EIS measurement, each sample was immersed in the corrosion cell and allowed to stabilize for 2 h. The EIS studies were performed by imposing a sinusoidal voltage of 10 mV amplitude as the open circuit potential of the working electrode. The frequency was varied between 0.1 Hz to 100 kHz. CV measurements at scan rates 100 mV/s were performed in the potential window of 0–0.8 V. The currents obtained for each electrode were divided by the mass of a corresponding graphene hydrogel.

2.2. Graphene oxide synthesis

Graphene oxide was synthesized using the improved Hummers method, described in our previous report [39]. Briefly, 2 g of graphite flakes was mixed with 6 g of $KMnO_4$. Then the mixture of H_2SO_4/H_3PO_4 (120 mL: 30 mL) was slowly added. An ice bath was used to keep the temperature below 5 °C. The suspension was left for 48 h with magnetic stirring and for the next 48 h in an ultrasonic bath. Then the mixture was diluted with distilled water and hydrogen peroxide (30%) was added in order to stop the reaction and reduce manganese (VII) ions. It resulted in a colour change to brown-yellow and graphite oxide was obtained. The suspension was centrifuged at 15000 rpm for 10 min and washed several times with deionized water. It was dried in a vacuum dryer at 30 °C for 2–3 days. To obtain GO, graphite oxide (4 mg mL^{-1}) was sonicated for 3–4 h.

2.3. Preparation of graphene hydrogels

Two well-known protocols for graphene hydrogels formation both in acidic and basic conditions were adapted in our experiments.

2.3.1. Ascorbic acid-assisted gelation of graphene oxide

In the first method, ascorbic acid (AA) was used in order to reduce graphene oxide aqueous dispersions at low temperature (90 °C). The reason for choosing AA was that it is a mild and environmentally friendly reducing agent that releases no gaseous by-products that could affect the pore creation. Different concentrations and volumes of the suspensions were used in order to study the influence of initial synthesis conditions on the hydrogel structure. GO suspension with concentration of 2 mg mL^{-1} was prepared and diluted subsequently to obtain a desired concentration. GO concentration of 2 mg mL^{-1} was chosen to study the effect of different GO volume (4, 6 and 9 mL). GO suspension volume of 9 mL was chosen to study the effect of different GO concentration (0.5, 1 and 2 mg mL^{-1}). The effect of pH was also studied. For acidic samples (AC), 1 μL of hydrochloric acid per 1 mL of suspension was added reaching pH ~2. Samples in basic conditions (BC) were prepared by adding 1 μL of ammonia per 1 mL of suspension reaching pH ~10. Different mass ratio of ascorbic acid to graphene oxide (namely 20:1 and 10:1, denoted as **20AA** and **10AA**, respectively) was used to study the effect of the reducing agent on the hydrogel structure. As-prepared 10 samples (5 per each pH condition) were sonicated in glass vials for 1 h and AA was added. The vials were capped tightly and heated at 90 °C for 2 h. As-formed hydrogels were washed several times and kept for several days in deionized water in order to remove any residual by-products and unreacted ascorbic acid. After characterization, they were put in ethanol for a few days for the solvent exchange. Supercritical drying was used in order to obtain aerogels with the same protocol for all samples.

2.3.2. Hydrothermal gelation in autoclave

In the second approach, the hydrothermal gelation of GO at higher temperatures (180 °C) was used using an autoclave (notation **Aut** was used for these samples). No ascorbic acid was added. GO suspension with concentration of 4 mg mL^{-1} was prepared and diluted subsequently to obtain a desired concentration. GO concentration of

4 mg mL^{-1} was chosen to study the effect of different GO volume (6, 9 and 12 mL). GO suspension volume of 12 mL was chosen to study the effect of different GO concentration (2, 3 and 4 mg mL^{-1}). The effect of pH was also studied with the same protocol as before (1 µL of ammonia/HCl per 1 mL of GO suspension). As-prepared 10 samples (5 per each pH condition) were placed in a Teflon-lined autoclave and kept for 8 h at 180 °C. As-formed hydrogels were washed several times with deionized water. After characterization, they were put in ethanol for a few days for the solvent exchange. Supercritical drying was used in order to obtain aerogels with the same protocol for all samples.

The notation of samples prepared by both methods is as follows. The hydrogel samples were denoted as **GHX_Y** where X corresponds to the initial GO concentration and Y to the volume of GO suspension. The aerogels were labelled as **GAX_Y** where X corresponds to the initial GO concentration and Y to the volume of GO suspension.

2.4. Gold nanoparticles synthesis and adsorption

Gold nanoparticles were synthesized using a chemical reduction method in water [40]. 30 mg of $HAuCl_4 \cdot xH_2O$ was added to 150 mL of distilled water and heated to boiling while stirring in a beaker. Then 1.8 mL of citric acid solution (50 mg mL^{-1}) was quickly added to the solution and the mixture was stirred for the next 2 h. The solution changed colour within several minutes from yellow to red. Chosen graphene hydro- and aerogels were immersed in the as- prepared Au nanoparticle solutions (40 mL) and stirred magnetically for 20 h. UV–vis spectra of Au nanoparticles solutions before samples immersion and after 20 h were collected and the mass of adsorbed nanoparticles (mg) per mass of graphene structure (in grams) were calculated (for more details, see Supporting Information).

3. Results and discussion

3.1. Structural characterization

A series of the well-defined cylindrically-shaped graphene hydrogels was successfully synthesized. Fig. 1 presents the pictures of chosen graphene hydrogels after synthesis.

It can be seen that hydrogels tend to replicate the shape and size of the vessel they are prepared in, which was also observed by others [41,42]. Hydrogel weights for all samples are listed in Table 1. Samples with 20AA have larger masses comparing to samples with 10AA. Moreover, hydrogels prepared in an autoclave have smaller masses and sizes than hydrogels prepared with the use of ascorbic acid. Both in AC and BC, the increase of GO concentration and the increase of GO suspension volume resulted in hydrogels of larger heights, with a negligible change in cylinder diameters. Therefore, the vessel shape and size have an influence on the final structure of graphene hydrogels. For the samples of the same initial parameters e.g. GA2_6 and GA2_9 (refer to Table 1) prepared by three different strategies (20AA, 10AA, Aut), the mass of a hydrogel increases with increasing the amount of AA. It can be concluded that the addition of AA significantly influences the weight of a hydrogel and ascorbic acid residues may be still present even after a few days of washing. It is known that when ascorbic acid is used as a supporting reducing agent, additional crosslinking can occur. Ascorbic acid ($C_6H_8O_6$) oxidizes to dehydroascorbic acid ($C_6H_6O_6$) which can be further converted to guluronic and oxalic acids [43,44]. Additionally CO_2, CO and water are created during GO reduction to RGO. The scheme of the reaction is shown in Fig. 2A. The formed by-products may form additional hydrogen bonds with residual carboxylic groups on reduced graphene oxide planes and contribute to the final mass of hydrogels. The cross-linking of hydrogel with organic moieties formed in the reaction is schematically depicted in Fig. 2B3. Moreover, the temperature during hydrothermal reaction is much higher (180 °C in autoclave and c.a. 90 °C in the AA assisted synthesis), causing deoxygenation of graphene oxide in a greater extent, leading to fragmentation of GO and in consequence, lower mass of GH-Aut samples.

The bulk density of aerogels was also determined (Table 1). For all samples, the calculated density was very low and ranged from 2.41 to 4.02 mg cm^{-3}. Aerogels prepared from lower GO concentration as well as from lower GO dispersion volume exhibit higher bulk density. These results are consistent with the literature data. Nguyen et al. [18] observed the lower bulk density (up to 63 mg cm^{-3}) for samples prepared from higher GO concentration (2, 3, 5 and 10 mg mL^{-1}). Similar behaviour was observed by Fan et al. [19].

3.2. Water content of graphene hydrogels

During the hydrothermal gelation, water molecules from aqueous dispersion are entrapped between reduced graphene oxide sheets via hydrogen bonds. Thus, the water content (WC) of each hydrogel was

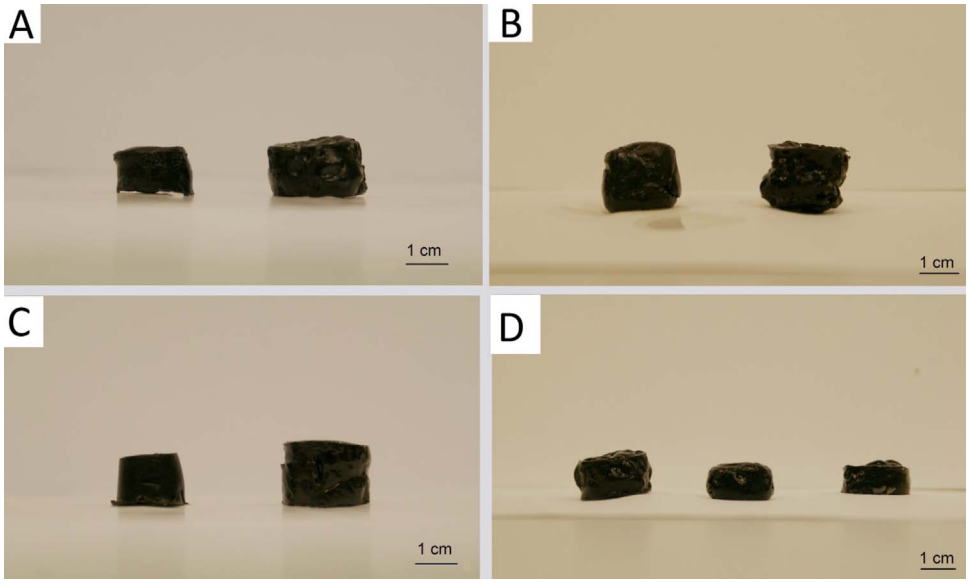

Fig. 1. Comparison of corresponding samples prepared in AC and BC. A. GA2_6 sample (20AA) prepared in acidic (left) and basic conditions (right). B. GA2_6 sample (10AA) prepared in acidic (left) and basic conditions (right). C. GA2_6 sample (Aut) prepared in acidic (left) and basic conditions (right). D. Chosen samples GA2_6 prepared in AC with 20AA (left), 10 AA (middle) and in an autoclave (right).

Table 1
Hydrogel mass and water content for all samples prepared in acidic and basic media.

Samples	Hydrogel mass (g)				Water content (%)				Bulk density (mg cm^{-3})			
	AC		BC		AC		BC		AC		BC	
	10AA	20AA	10AA	20AA	10AA	20AA	10AA	20AA	10AA	20AA	10AA	20AA
GH0.5_9	0.335	0.381	0.361	0.393	99.328	99.408	99.395	99.427	3.77	3.56	3.21	3.16
GH1_9	0.768	0.819	0.806	0.883	99.414	99.450	99.432	99.490	3.69	3.12	3.04	3.01
GH2_9	1.669	1.982	1.712	2.059	99.460	99.546	99.474	99.563	3.64	2.86	2.97	2.63
GH2_6	1.043	1.250	1.128	1.345	99.425	99.520	99.468	99.554	3.54	2.61	3.52	2.41
GH2_4	0.676	0.818	0.717	0.878	99.408	99.511	99.442	99.544	4.02	2.98	3.91	2.73

	AC	BC	AC	BC	AC	BC
GH2_6	0.435	0.474	98.620	98.735	12.75	10.59
GH2_9	0.699	0.886	98.714	98.984	11.42	9.98
GH2_12	1.065	1.608	98.873	99.254	11.96	10.21
GH3_12	1.417	2.006	98.731	99.103	11.67	9.34
GH4_12	1.761	2.228	98.683	98.923	8.43	7.67

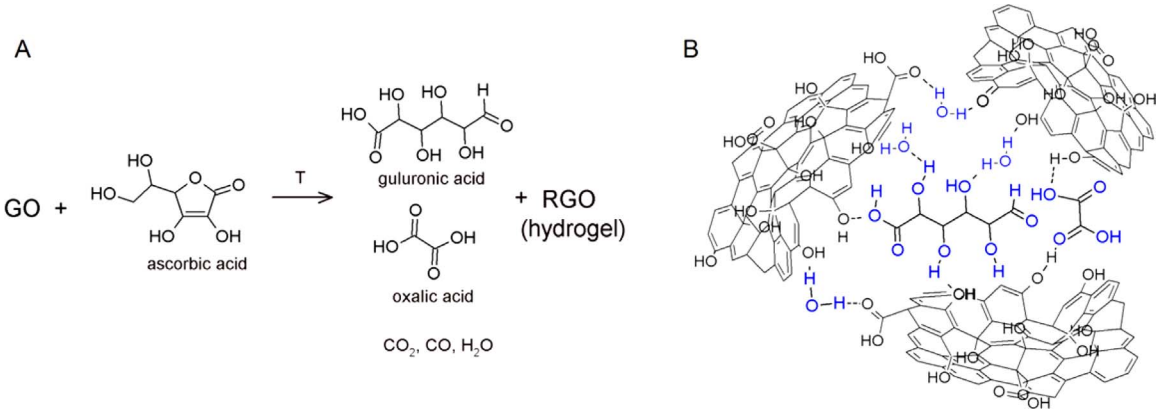

Fig. 2. A. Scheme of the redox reaction between GO and AA leading to the hydrogel formation and creation of various by-products, B. Cross-linking of the hydrogel with organic fragments released upon AA oxidation.

calculated using the following formula:

$$WC = \frac{m_{hydrogel} - m_{foam}}{m_{hydrogel}} \quad (1)$$

The results are presented in Table 1. The results show that hydrogels prepared by AA-assisted reduction have WC in the range of 99.328–99.563%. Samples prepared in an autoclave exhibit lower water content (98.620–99.254%). This may be connected with higher temperature and pressure in the autoclave. As the deoxygenation of GO occurs in a greater extent, the number of residual oxygen groups is smaller than in AA-reduced GO. Water molecules can be entrapped in the voids formed in the hydrogel and can be additionally retained by hydrogen bonding formation. If there are less functional groups in the autoclave- prepared hydrogel, there are simultaneously less water molecules forming hydrogen bonds with them. We also observed that an increase in GO concentration and GO volume resulted in an increase of WC both for samples prepared in AC and BC. In the studies performed by Xu et al. [15] water content of hydrogels prepared using 10 mL of GO (0.5, 1 and 2 mg mL^{-1}) was found to be in the range of 97–99% whereas Cerruti et al. [16] reported water content of hydrogels (10 mL, 4 mg mL^{-1}) prepared by hydrothermal method to be above 98%. Many recent studies revealed that the pH of the GO suspension can have an impact on the final structure of hydrogels. According to the study carried out by [16,45,46], during the hydrothermal reduction of GO, carbon dioxide, carbon monoxide, water, and organic fragments are released. Moreover, the gaseous products release strongly depends on the pH of the GO suspension and it can have a substantial impact on the final structure of hydrogels. When the hydrogel formation proceeds at pH $<$ 7, gaseous CO_2 is trapped between the graphene sheets and thus contributes to the creation of macroscopic voids inside the hydrogel. On the other hand, if the hydrothermal reduction is carried out in the basic media, CO_2 reacts with water to form carbonic acid, and no gas bubbles are formed. Based on these studies, it can be suggested that CO_2 bubbles that form in acidic media may also have an impact on the water entrapment inside the hydrogel. Furthermore, our experiments showed that samples prepared in BC exhibited slightly higher water content when compared to the corresponding samples prepared in AC. The same tendency was observed by Xie et al. [17]. Their studies showed that with increasing pH (from 1.65–11.73), the water content of hydrogels (10 mL, 3 mg mL^{-1}) increased from 97.6% to 98.6%. Interestingly, as shown in the previous section, samples prepared in BC were about 50% larger in volume than those prepared in AC (Fig. 1). The reason for this can be also connected with CO_2 bubbles release. For samples prepared in BC they form carbonic acid that can fill the hydrogel voids with water, resulting in higher volume and water content.

3.3. Morphology and surface characterization of graphene aerogels

The outer surface areas of the prepared GAs were imaged using scanning electron microscopy (SEM). Fig. S1 shows the morphology of graphene oxide that composes of thin, folded layers. SEM images of the chosen GA2_6 sample prepared by three different strategies are shown in Fig. S4. All aerogels exhibit well-developed outer surface area with non-uniformly distributed micrometre-sized pores. The images clearly demonstrate that all aerogels are composed of thin, few-layered

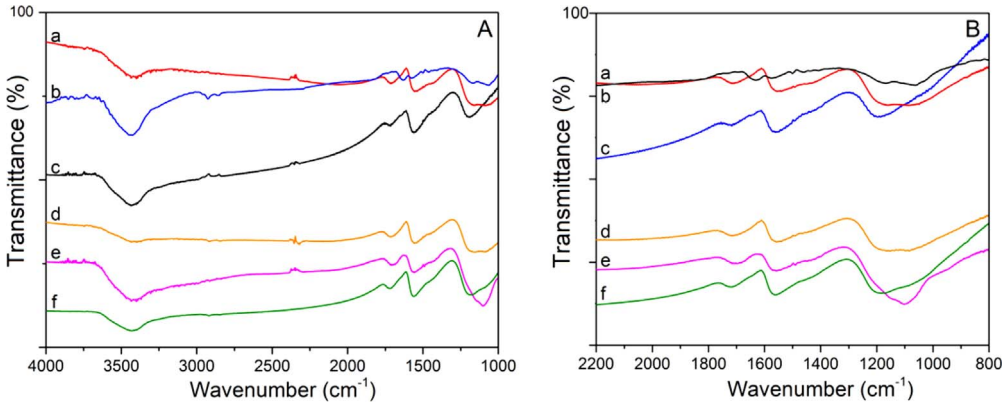

Fig. 3. A. FTIR spectra of a chosen GA2_6 sample prepared in different conditions (a) 20AA, AC, (b) 20AA, BC (c) 10AA, AC (d) 10AA, BC (e) Aut, AC (f) Aut, BC. B. FTIR spectra in the range of 2200–800 cm^{-1}.

reduced graphene oxide sheets, interconnected with each other forming a porous wrinkled surface. GAs prepared in acidic media exhibit many visible voids and well-developed, porous surface in comparison to the sample prepared in BC. In this case, a smooth surface was observed. In addition, the pores on the surface in case of GA prepared in AC can originate from the CO_2 bubbles, suggesting that gas may be also entrapped on the surface.

FTIR spectroscopy was used to determine different functional groups present on graphene plane. The FTIR spectrum of GO (Fig. S2) shows several bands that can be ascribed to various oxygen functionalities. In contrast, the FTIR spectra of graphene aerogels (Fig. 3) show a considerable reduction in the oxygen containing functional groups confirming the deoxygenation. However, no significant differences can be observed between different GAs spectra. A band centred at c.a. 3390 cm^{-1} together with a distinct band at 1644 cm^{-1} can be assigned to O—H vibrations of water molecules adsorbed on aerogels. Distinct band at 1735 cm^{-1} confirms the presence of carbonyl C═O groups which were not fully removed after reduction. The band at 1590 cm^{-1} is assigned to the stretching vibrations of C═C conjugated with C═C or C═O bonds. A broad band at about 1000–1200 cm^{-1} is placed in the region characteristic for stretching of C—O bonds in alcohols and epoxides that still remain in the samples.

3.4. Surface area measurements

The methylene blue (MB) adsorption method was used to determine the specific surface area of graphene hydrogels (MB surface area) after synthesis. BET surface area and total pore volume analysis was used to determine the surface area of graphene aerogels. All the results are presented in Table 2. Graphene hydrogels exhibit MB surface area in the range of 230–2015 $m^2\,g^{-1}$ for those prepared in acidic media and 250–2200 $m^2\,g^{-1}$ for GHs prepared in basic conditions. BET surface area of graphene aerogels was found to be in the range of 411–578 $m^2\,g^{-1}$ (total pore volume 0.201–0.283 cm^3) for those prepared in acidic media and 502–645 $m^2\,g^{-1}$ (total pore volume 0.218–0.305 cm^3) for GAs prepared in basic conditions. These values are lower than in MB adsorption method used for hydrogels, suggesting that after supercritical drying the accessible surface area decreases, due to the slight shrinkage of hydrogels volume. The effect of GO initial concentration and volume on the specific surface area of hydrogels and aerogels was studied. When increasing the initial GO concentration, surface area of graphene materials was found to decrease (Fig. 4A). Similarly, an increase in GO suspension volume resulted in a decrease of surface area (Fig. 4B). As expected, higher concentration of GO dispersion causes more pronounced stacking of graphene sheets, therefore hinders the accessible surface area for adsorption. This correlation was also studied in the literature [14,15,18,19]. Moreover, hydrogels prepared in BC possess higher surface area than corresponding samples prepared in AC. Similar behaviour but lower surface area values were observed by Bai et al. [13]. In this study, the MB surface area was the highest for the hydrogels prepared in basic media (pH═10) in comparison to samples prepared in neutral and acidic media and was equal to 480 $m^2\,g^{-1}$. Xie et al. [17] found the surface area of hydrogels to be in the range of 723.35 $m^2\,g^{-1}$ to 1107.24 $m^2\,g^{-1}$, with the highest value for the hydrogel prepared in basic media (pH═11.73). To explain these results, the behaviour of GO in aqueous media needs to be analysed. It is known that GO possesses carboxylic groups that are ionized and therefore repulse single GO sheets, preventing the aggregation in water [46]. Upon adding an acid the repulsion is weakened, whereas adding a base resulted in an increase in the repulsion force and more stable GO dispersion. Due to this phenomena, more aggregated graphene sheets are observed on the surface of GAs prepared in AC, and, contrary, more separated sheets compose the surface of GAs in BC. So in more loosely-oriented RGO flakes (in BC), more room is available for MB molecules, thus the specific surface area is higher. Moreover, CO_2 bubbles that are present in GHs prepared in AC can also hinder the accessible surface area.

By comparing the specific surface areas of the samples prepared by three different strategies but from the same GO concentration and volume (highlighted in Table 2), it can be seen that the highest values are observed for hydro- and aerogels prepared in an autoclave, without the addition of ascorbic acid. The reason may be higher temperature and pressure that affect the self-assembly process. Temperature was found to play an important role in sol-gel process used to produce SiO_2 nanoparticles [47]. The dimensions of synthesized nanoparticles were decreasing with increasing the temperature. Similar behaviour is possible in the case of GO gelation process. In the higher temperature smaller packages of GO are formed, which next organize into 3D structure. If the building blocks are smaller, it may result in higher amount of pores created inside the hydrogels and consequently, higher specific surface area as compared to hydrogels prepared with AA. Moreover, with the use of autoclave no additional crosslinkers are used, simplifying the synthesis method. Therefore, those samples were chosen for further experiments.

3.5. XRD studies

XRD measurements were carried out to analyse the layer-to-layer distance (d-spacing) between graphene sheets and the main crystalline size (that is a height of the stacked RGO layers) in GAs. All data are presented in Table 3. The Bragg's equation was applied to calculate the distance (d) between RGO layers in different samples. The Scherrer's equation with a constant k = 0.9 was applied for evaluating the average height of stacked layers, denoted as H. A number of stacked graphene layers was also evaluated.

Table 3 shows the structural parameters of samples, as measured by

Table 2
Synthesis parameters and characteristics of samples prepared in acidic (AC) and basic (BC) conditions.

Samples	BET surface area ($m^2 g^{-1}$)		Total pore volume ($cm^3 g^{-1}$)		Samples	MB surface area ($m^2 g^{-1}$)	
	AC	BC	AC	BC		AC	BC
20AA					**20AA**		
GA0.5_9	496.8	522.1	0.222	0.242	**GH0.5_9**	763.2	842.1
GA1_9	470.0	489.9	0.209	0.225	**GH1_9**	586.6	658.6
GA2_9	411.3	502.6	0.201	0.218	**GH2_9**	482.5	513.4
GA2_6	454.5	506.7	0.217	0.233	**GH2_6**	526.5	657.7
GA2_4	518.2	632.4	0.265	0.287	**GH2_4**	876.2	959.9
10AA					**10AA**		
GA5_9	502.3	531.7	0.230	0.257	**GH5_9**	888.6	925.2
GA1_9	471.8	519.9	0.215	0.243	**GH1_9**	706.6	796.8
GA2_9	425.3	514.4	0.206	0.229	**GH2_9**	578.3	618.6
GA2_6	481.5	520.7	0.228	0.252	**GH2_6**	923.8	1248.3
GA2_4	561.7	632.4	0.271	0.297	**GH2_4**	1605.4	1762.3
Aut					**Aut**		
GA2_6	578.9	645.8	0.283	0.305	**GH2_6**	1101.3	1612.2
GA2_9	514.2	570.6	0.235	0.267	**GH2_9**	627.2	952.6
GA2_12	490.3	531.7	0.231	0.261	**GH2_12**	503.3	691.1
GA3_12	481.4	525.0	0.222	0.249	**GH3_12**	319.2	358.5
GA4_12	434.3	524.9	0.214	0.238	**GH4_12**	230.1	257.0

XRD. As compared to the XRD spectrum of GO (Fig. S2), the removal of functional groups led to the decrease in the interlayer spacing, from 0.863 nm for GO to 0.351–0.377 nm for different GA samples and it was slightly higher than that of graphite (0.336 nm). This suggests that oxygen functionalities are still present on graphene planes. The broad XRD signals of the GAs (Fig. 5) indicated the poor ordering of reduced graphene oxide sheets along their stacking direction. Moreover, the structure of the GAs is composed of the few-layer stacked RGO sheets, which was consistent with the results obtained by SEM. It was found that slightly smaller interlayer spacing can be observed for samples prepared in basic conditions (BC) comparing to the samples prepared in acidic conditions. The largest interlayer spacing for samples prepared both in AC and BC is observed for GA2_12, whereas the smallest for GA2_6 sample. The height of stacking GO layers was found to be 15.12 nm and decreased to 2.02–3.93 nm for GAs prepared in AC and to 1.98–3.81 nm for samples prepared in BC. The number of layers was calculated to be 17 for pristine GO and decreased to 5–10 layers for all graphene aerogels samples. As mentioned previously, more aggregated graphene sheets are observed on the surface of GAs prepared in AC, whereas separated sheets compose the surface of GAs prepared in BC. However, due to the presence of CO_2 bubbles in the structure of GHs prepared in AC, graphene sheets may be separated from each other and larger interlayer spacing is observed in case of AC, which also agree with other reported studies [13,48].

Table 3
Structural parameters of chosen GA samples, as studied by XRD diffraction. Notation: d-average distance between RGO stacking layers (d-spacing), according to the Bragg's law, H- height of the stacked graphene layers, according to the Scherrer's method, *n*- number of graphene stacking layers.

Samples	2θ (°)		d (nm)		H (nm)		n	
	AC	BC	AC	BC	AC	BC	AC	BC
GA2_6	25.35	26.40	0.351	0.337	3.29	3.17	9.37	9.38
GA2_9	24.96	24.66	0.356	0.361	2.78	2.70	7.81	7.49
GA2_12	23.61	24.38	0.377	0.365	3.93	3.81	10.44	10.44
GA3_12	23.78	24.46	0.374	0.364	2.26	2.25	6.03	6.19
GA4_12	24.40	24.65	0.365	0.361	2.02	1.98	5.55	5.49

3.6. Electrochemical studies

The electrochemical properties of hydrogels prepared in an autoclave were studied by cyclic voltammetry (CV) and electrochemical impedance spectroscopy (EIS). Fig. 6A shows the CV curves of hydrogels GH_AUT in the range of 0–0.8 V vs SCE at the scan rate of 100 mV/s. Supercapacitors based on GHs exhibit similar CV behaviour, due to the very porous internal and external structure. Hydrogels GH2_12, GH3_12 and GH4_12 show better EDLC characteristics (See curves c–e) than samples GH2_6 and GH2_9 (curves a and b). However, for the latter, bigger integral areas are found which means that the specific capacitances of the GH2_6 and GH2_9 are higher. This result can be ascribed to the interconnected porous structures with higher surface

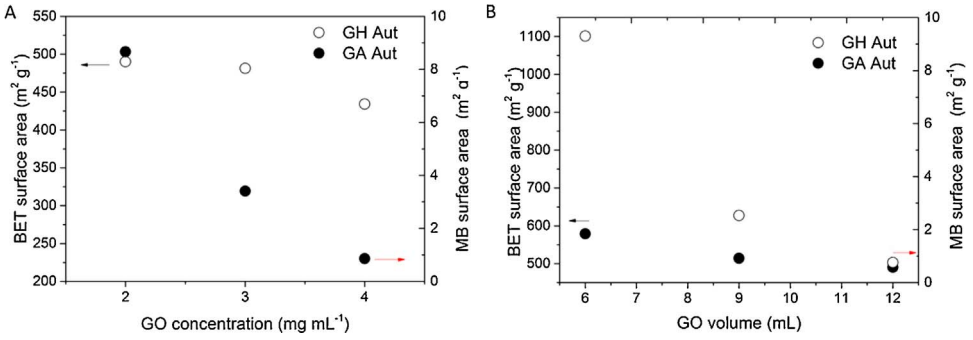

Fig. 4. MB surface area and BET surface area vs GO concentration (A) and volume (B) for GH Aut and GA Aut samples, respectively.

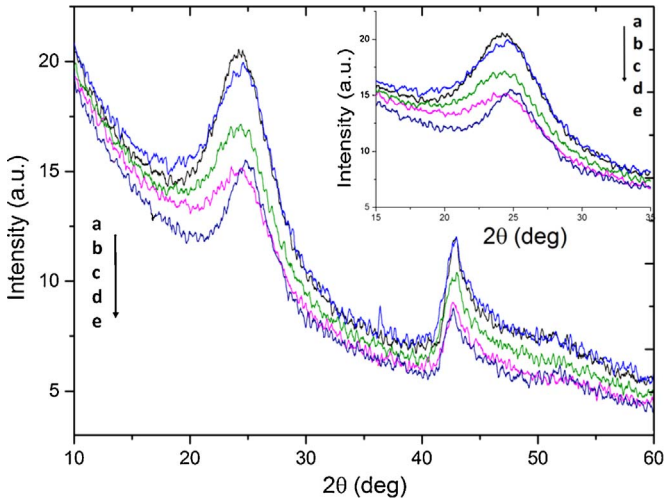

Fig. 5. XRD patterns of dried hydrogels prepared in acidic conditions: a. GA2_6, b. GA2_9, c. GA2_12, d. GA3_12 e. GA4_12.

area that could enhance electron and ion diffusion. This is in agreement with adsorption studies showing higher surface areas for samples prepared with smaller GO volume and smaller GO concentration (GH2_6 and GH2_9).

Impedance measurements of the studied electrode at its open circuit potential upon instant immersion in H_2SO_4 solution were carried out in order to obtain information about the kinetics of different graphene hydrogels. The Nyquist plots are shown in Fig. 6B. All plots revealed a typical response of porous structures. The semicircle in the high-frequency range is associated with the charge-transfer resistance, and a nearly vertical line at low frequency indicates a capacitive behaviour of electrochemical double-layer capacitor. The EIS data were fitted on the basis of the equivalent circuit using ZSimpWin 3.21 software as shown on the inset in Fig. 4B. R_e is the electrolyte resistance between the working and reference electrodes, R_f and Q refers to resistance and double layer capacitance components of electrode porosity response, R_{ct} is the charge transfer resistance and C is the capacitance element. GH4_12 and GH3_12 was found to possess the lowest charge-transfer resistance (225 and 560 Ω, respectively) in comparison to samples GH2_6 and GH2_9 (about 734 and 1250 Ω, respectively). This may indicate that samples prepared from more concentrated GO dispersion possess lower charge transfer resistance which is probably due to the more interconnected carbon network facilitating the charge transfer between the sample and the electrolyte. Furthermore, a nearly vertical line can be observed on the Nyquist plot of the graphene hydrogels, owing to a supercapacitive behaviour of graphene hydrogels.

Table 4
Au NP adsorption ($mg \cdot g^{-1}$) of chosen graphene hydro- and aerogels.

Samples	Au NP adsorption (10^{-5} mg g^{-1})			
	Hydrogels		Aerogels	
	AC	BC	AC	BC
G2_6	103.5	92.3	90.8	53.2
G2_9	53.2	48.3	46.3	42.5
G2_12	59.8	55.6	45.3	44.2
G3_12	4.2	1.9	4.1	1.2
G4_12	2.1	0.7	1.3	0.5

3.7. Gold nanoparticles adsorption

The adsorption ability of graphene hydro- and aerogels was determined by recording UV–vis spectra of pure gold nanoparticles solution and solution after 20 h of samples immersion. SEM image of gold nanoparticles and detailed description of the experiment are shown in Supporting Information. The obtained results are shown in Table 4. It can be seen that the highest adsorption ability ($103.5 \cdot 10^{-5}$ mg/g) was found for GH2_6 prepared in AC which exhibited the highest surface area among other samples prepared in AC. Samples GH2_9 and GH2_12 show similar sorption ability but noticeably lower than GH2_6 sample. The values for all hydrogels prepared in BC were slightly lower in comparison to hydrogels prepared in AC. The Au nanoparticles adsorption mechanisms is still not clear and requires further investigations. It is known that the mechanism responsible for the adsorption of metallic nanoparticles on carbonaceous materials is complex and includes electrostatic, van der Waals, hydrophobic, π–π stacking, hydrogen bonding etc [48]. Some studies show that the affinity of gold nanoparticles for carbon-based materials is governed by the interplay between those non-covalent interactions (that can be changed by pH of the reaction environment) as well as the size of nanostructures (nanoparticle diameter, size of graphene sheets, height of stacking layers etc.) [49]. XRD measurements (shown previously) confirmed that hydrogels prepared in AC exhibited slightly larger interlayer spacing and height of stacking layers which may be favourable for adsorption of gold nanoparticles of a certain size (in this case 25 nm). Moreover, GHs are preferable for Au NPs adsorption over GAs. This was also confirmed by SEM images with EDS analysis (Fig. 7, Table S1) showing that the%weight of Au on the hydro- and aerogel surface was 18% and 3%, respectively. It is most likely due to the hydrophobicity of graphene aerogels which hinders the adsorption of Au nanoparticles from aqueous solution. The relation between Au nanoparticles adsorption and surface area of hydro- and aerogels was presented in Fig. 8.

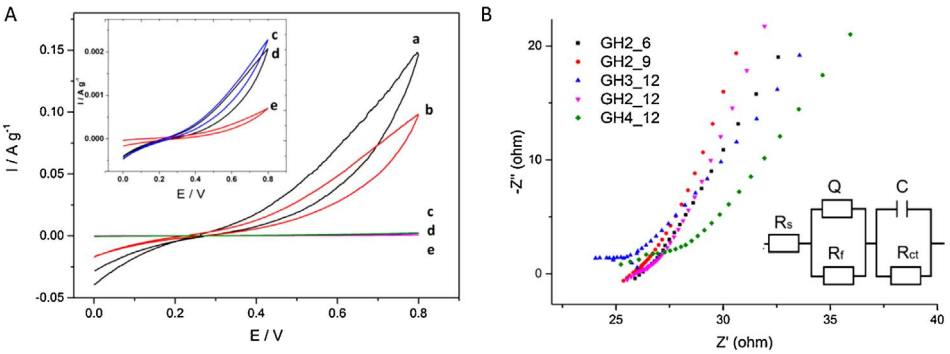

Fig. 6. A. Cyclic voltammograms for hydrogels (Aut, AC) at scan rate of 100 mV/s a. GH2_6, b. GH2_9, c. GH2_12, d. GH3_12 e. GH4_12. Inset: Voltammograms c, d, e. B. Nyquist plots for chosen graphene hydrogels (Aut, AC). Inset shows the equivalent circuit used for fitting the impedance spectra.

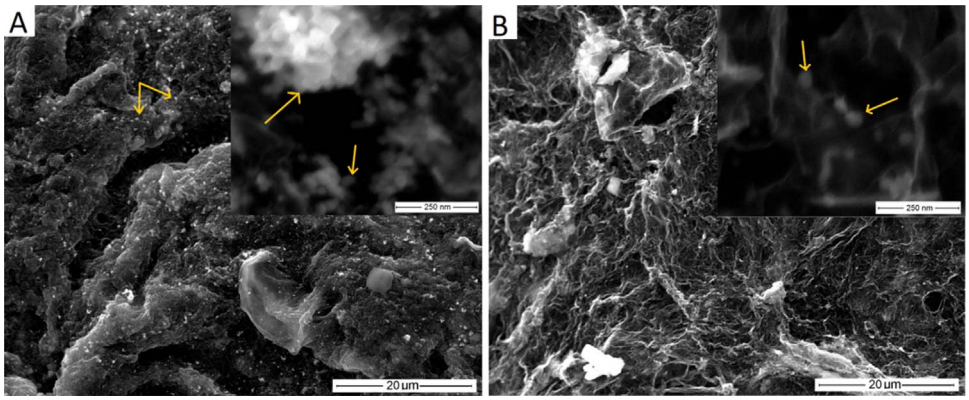

Fig. 7. SEM images of A. dried graphene hydrogel and B. graphene aerogel after gold nanoparticles adsorption. Arrows point gold nanoparticles. Scale 20 µm. Inset: Scale 250 nm.

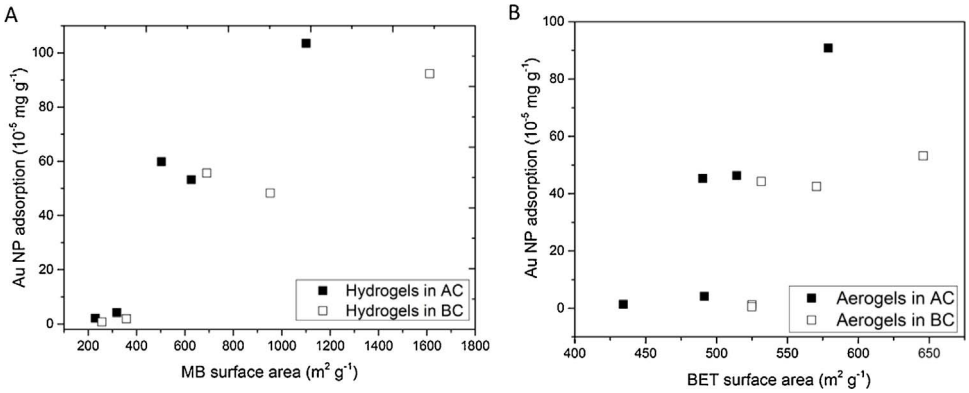

Fig. 8. A. Au NP adsorption vs. MB surface area for graphene hydrogels and B. Au NP adsorption vs. BET surface area for graphene aerogels prepared in AC anc BC.

4. Conclusions and future prospects

In this work graphene hydrogels and aerogels were prepared by chemically-assisted and hydrothermal gelation of GO aqueous dispersion both in acidic and basic media. The hydrogels size, bulk density, water content, specific surface area and, in consequence, the adsorption properties strongly depend on the synthesis parameters, including temperature, pressure, the usege of reducing agent, as well as concentration and volume of graphene oxide suspension. Graphene hydrogels and aerogels manufactured in autoclave exhibit high surface areas of 250–2000 $m^2\ g^{-1}$ as determined by MB adsorption method and BET surface areas ranging from 500 to 640 $m^2\ g^{-1}$ after supercritical drying, respectively. Adsorption ability of graphene hydro- and aerogels towards gold nanoparticles was evaluated. The highest sorption ability of $103.5{\cdot}10^{-5}$ mg g^{-1} was recorded for the hydrogel with the highest surface area. Further investigation of nanoparticles adsorption on graphene hydro- and aerogels will be performed including the adsorption kinetics and adsorption mechanisms of nanoparticles with different size and shape.

Acknowledgements

Authors would like to thank Anna Zielińska-Jurek's group (Department of Chemical Technology, Faculty of Chemistry, GUT) for the help with BET measurements.

Appendix A. Supplementary data

Supplementary data associated with this article can be found, in the online version, at http://dx.doi.org/10.1016/j.colsurfa.2017.05.063.

References

[1] X. Dong, X. Wang, L. Wang, H. Song, H. Zhang, W. Huang, P. Chen, 3D graphene foam as a monolithic and macroporous carbon electrode for electrochemical sensing, ACS Appl. Mater. Interfaces 4 (2012) 3129–3133, http://dx.doi.org/10.1021/am300459m.

[2] D.A.C. Brownson, L.C.Z. Figueiredo-Filho, X. Ji, M. Gomez-Mingot, J. Iniesta, O. Fatibello-Filho, D.K. Kampourisa, C.B. Banks, Freestanding three-dimensional graphene foam gives rise to beneficial electrochemical signatures within non-aqueous media, J. Mater. Chem. A 1 (2013) 5962, http://dx.doi.org/10.1039/C3TA10727B.

[3] Y. Zhong, Z. Mi, F. Huang, T. Lin, D. Wan, Effect of graphene aerogel on thermal behavior of phase change materials for thermal management, Sol. Energy Mater. Sol. C 113 (2013) 195–200, http://dx.doi.org/10.1016/j.solmat.2013.01.046.

[4] C.C. Ji, M.W. Xua, S.J. Bao, C.J. Cai, Z.J. Lu, H. Chai, F. Yang, H. Wei, Self-assembly of three-dimensional interconnected graphene-based aerogels and its application in supercapacitors, J. Colloid Interface Sci 407 (2013) 416–424, http://dx.doi.org/10.1016/j.jcis.2013.06.054.

[5] I. Kondratowicz, K. Żelechowska, D. Majdecka, R. Bilewicz, Synthesis and modification of reduced graphene oxide aerogels for biofuel cell applications, Mat. Sci. Poland 33 (2015) 292–300, http://dx.doi.org/10.1515/msp-2015-0042.

[6] K. Żelechowska, B. Trawiński, S. Dramińska, D. Majdecka, R. Bilewicz, B. Kusz, Oxygen biosensor based on carbon nanotubes directly grown on graphitic substrate, Sens. Actuators B: Chem. 240 (2017) 1308–1313, http://dx.doi.org/10.1016/j.snb.2016.09.081.

[7] P. Liu, Z. Fan, A. Mikhalchan, T. Tran, D. Jewell, H. Duong, A. Marconnet, Continuous carbon nanotube-based fibers and films for applications requiring enhanced heat dissipation, ACS Appl. Mater. Interfaces 8 (2016) 17461–17471, http://dx.doi.org/10.1021/acsami.6b04114.

[8] T. Tran, Z. Fan, P. Liu, H. Duong, Advanced morphology-controlled manufacturing of carbon nanotube fibers, thin films and aerogels from aerogel technique, Asia Pacific Confederation of Chemical Engineering Congress 2015: APCChE 2015, Incorporating CHEMECA 2015, Melbourne : Engineers Australia, 2015, pp. 2444–2451 (ISBN: 9781922107473).

[9] H. Duong, F. Gong, P. Liu, T. Tran, Advanced fabrication and properties of aligned carbon nanotube composites: experiments and modeling, Carbon Nanotube –Curr. Progress Polym. Compos. Intech (2015) 47–72, http://dx.doi.org/10.5772/62510.

[10] H. Cheng, P. Kohl, P. Liu, T. Tran, H. Duong, Continuous self-assembly of carbon nanotube thin films and their composites for supercapacitors, Colloid Surf. A 481 (2015) 626–632, http://dx.doi.org/10.1016/j.colsurfa.2015.06.039.

[11] Y. Ding, J. Zhu, C. Wang, B. Dai, Y. Li, Y. Qin, F. Xu, Q. Peng, Z. Yang, J. Bai, W. Cao, Y. Yuan, Y. Li, Multifunctional three-dimensional graphene nanoribbons

composite sponge, Carbon 104 (2016) 133–140, http://dx.doi.org/10.1016/j.carbon.2016.03.058.
[12] S. Nardecchia, D. Carriazo, M.L. Ferrer, M.C. Gutierrez, F. del Monte, Three dimensional macroporous architectures and aerogels built of carbon nanotubes and/or graphene: synthesis and applications, Chem. Soc. Rev. 42 (2013) 794, http://dx.doi.org/10.1039/C2CS35353A.
[13] B. Yaocai, R.B. Rakhi, W. Chen, H.N. Alshareef, Effect of pH-induced chemical modification of hydrothermally reduced graphene oxide on supercapacitor performance, J. Power Sources 233 (2013) 313–319, http://dx.doi.org/10.1016/j.jpowsour.2013.01.122.
[14] H.N. Lim, N.M. Huang, S.S. Lim, I. Harrison, C.H. Chia, Fabrication and characterization of graphene hydrogel via hydrothermal approach as a scaffold for preliminary study of cell growth, Int. J. Nanomed. 6 (2011) 1817–1823, http://dx.doi.org/10.2147/IJN.S23392.
[15] Y. Xu, K. Sheng, C. Li, G. Shi, Self-assembled graphene hydrogel via a one-step hydrothermal process, ACS Nano 4 (2010) 4324–4330, http://dx.doi.org/10.1021/nn101187z.
[16] K. Hu, X. Xie, T. Szkopek, M. Cerruti, Understanding hydrothermally reduced graphene oxide hydrogels: from reaction products to hydrogel properties, Chem. Mater. 28 (6) (2016) 1756–1768, http://dx.doi.org/10.1021/acs.chemmater.5b04713.
[17] Y. Xie, X. Sheng, X. Delong, L. Zixian, Z. Xinya, L. Zhong, Fabricating graphene hydrogels with controllable pore structure via one-step chemical reduction process, Carbon 109 (2016) 673–680, http://dx.doi.org/10.1016/j.carbon.2016.08.079.
[18] S.T. Nguyen, H.T. Nguyen, A. Rinaldi, N.P.V. Nguyen, Z. Fan, H.M. Duong, Morphology control and thermal stability of binderless-graphene aerogels from graphite for energy storage applications, Colloid Surf. A 414 (2012) 352–358, http://dx.doi.org/10.1016/j.colsurfa.2012.08.048.
[19] Z. Fan, D. Zhi Yong Tng, S.T. Nguyen, J. Feng, C. Lin, P. Xiao, L. Lu, H.M. Duong, Morphology effects on electrical and thermal properties of binderless graphene aerogels, Chem. Phys. Lett. 561–562 (2013) 92–96, http://dx.doi.org/10.1016/j.cplett.2013.01.033.
[20] X.H. Xia, D.L. Chao, Y.Q. Zhang, Z.X. Shen, Three-dimensional graphene and their integrated electrodes, Nano Today 9 (2014) 785–807, http://dx.doi.org/10.1016/j.nantod.2014.12.001.
[21] J.N. Tiwari, K. Mahesh, N.H. Le, K. Christian Kemp, R. Timilsina, R.N. Tiwari, K.S. Kim, Reduced graphene oxide-based hydrogels for the efficient capture of dye pollutants from aqueous solutions, Carbon 56 (2013) 173–182, http://dx.doi.org/10.1016/j.carbon.2013.01.001.
[22] J. Li, H. Meng, S. Xie, B. Zhang, L. Li, H. Ma, J. Zhanga, M. Yua, Ultra-light, compressible and fire-resistant graphene aerogel as a highly efficient and recyclable absorbent for organic liquids, J. Mater. Chem. A 2 (2014) 2934, http://dx.doi.org/10.1039/C3TA14725H.
[23] W. Peng, H. Li, Y. Liu, S. Song, A review on heavy metal ions adsorption from water by graphene oxide and its composites, J. Mol. Liq. 230 (2017) 496–504, http://dx.doi.org/10.1016/j.molliq.2017.01.064.
[24] J. Wang, B. Chen, Adsorption and coadsorption of organic pollutants and a heavy metal by graphene oxide and reduced graphene materials, Chem. Eng. J. 281 (2015) 379–388, http://dx.doi.org/10.1016/j.cej.2015.06.102.
[25] H. Huang, T. Chen, X. Liu, H. Ma, Ultrasensitive and simultaneous detection of heavy metal ions based on three-dimensional graphene-carbon nanotubes hybrid electrode materials, Anal. Chim. Acta 852 (2014) 45–54, http://dx.doi.org/10.1016/j.aca.2014.09.010.
[26] V.K. Gupta, S. Agarwal, A.K. Bharti, H. Sadegh, Adsorption mechanism of functionalized multi-walled carbon nanotubes for advanced Cu (II) removal (in press) http://dx.doi.org/10.1016/j.molliq.2017.01.083.
[27] R. Zare-Dorabei, S.M. Ferdowsi, A. Barzin, A. Tadjarodi, Highly efficient simultaneous ultrasonic-assisted adsorption of Pb(II), Cd(II), Ni(II) and Cu (II) ions from aqueous solutions by graphene oxide modified with 2,20-dipyridylamine: central composite design optimization, Ultrason. Sonochem. 32 (2016) 265–276, http://dx.doi.org/10.1016/j.ultsonch.2016.03.020.
[28] Y. Zhang, Y. Liu, X. Wang, Z. Sun, J. Ma, T. Wu, F. Xing, J. Gao, Porous graphene oxide/carboxymethyl cellulose monoliths, with highmetal ion adsorption, Carbohyd. Polym. 101 (2014) 392–400, http://dx.doi.org/10.1016/j.carbpol.2013.09.066.
[29] L.P. Lingamdinnea, Y.L. Choi, I.S. Kimb, J.K. Yang, J.R. Kodurub, Y.Y. Chang, Preparation and characterization of porous reduced graphene oxide based inverse spinel nickel ferrite nanocomposite for adsorption removal of radionuclides, J. Hazard. Mater. 326 (2017) 145–156, http://dx.doi.org/10.1016/j.jhazmat.2016.12.035.
[30] S. Goswami, P. Banerjee, S. Datta, A. Mukhopadhayay, P. Das, Graphene oxide nanoplatelets synthesized with carbonized agro-waste biomass as green precursor and its application for the treatment of dye rich wastewater, Process Saf. Environ. 106 (2017) 163–172, http://dx.doi.org/10.1016/j.psep.2017.01.003.
[31] M. Heidarizad, S.S. Şengör, Synthesis of graphene oxide/magnesium oxide nanocomposites with high-rate adsorption of methylene blue, J. Mol. Liq. 224 (2016) 607–617, http://dx.doi.org/10.1016/j.molliq.2016.09.049.
[32] Z. Zhang, F. Xiao, Y. Guo, S. Wang, Y. Liu, One-pot self-assembled three-dimensional TiO_2-graphene hydrogel with improved adsorption capacities and photocatalytic and electrochemical activities, ACS Appl. Mater. Interfaces 5 (2013) 2227–2233, http://dx.doi.org/10.1021/am303299r.
[33] Y. Yang, C.L. Long, H.P. Li, Q. Wang, Z.G. Yang, Analysis of silver and gold nanoparticles in environmental water using single particle-inductively coupled plasma-mass spectrometry, Sci. Total. Environ. 563–564 (2016) 996–1007, http://dx.doi.org/10.1016/j.scitotenv.2015.12.150.
[34] S.P. Mandyla, G. Tsogas, A.G. Vlessidis, D.L. Giokas, Determination of gold nanoparticles in environmental water samples by second-order optical scattering using dithiotreitol-functionalized CdS quantum dots after cloud point extraction, J. Hazard. Mater. 323 (2017) 67–74, http://dx.doi.org/10.1016/j.jhazmat.2016.03.039.
[35] B. Nowacka, J.F. Ranville, S. Diamond, J.A. Gallego-Urrea, C. Metcalfe, J. Rose, N. Horne, A.A. Koelmans, S.J. Klaine, Potential scenarios for nanomaterials release and subsequent alteration in the environment, Environ. Toxicol. Chem. 31 (2012) 50–59, http://dx.doi.org/10.1002/etc.726.
[36] Q. Sun, Y. Li, T. Tang, Z. Yuan, C.P. Yu, Removal of silver nanoparticles by coagulation processes, J. Hazard. Mater. 261 (2013) 414–420, http://dx.doi.org/10.1016/j.jhazmat.2013.07.066.
[37] D.F. Lawler, A.M. Mikelonis, I. Kim, B.L.T. Lau, S. Youn, Silver nanoparticle removal from drinking water: flocculation/sedimentation or filtration, Water Sci. Techol.: Water Supply 13.5 (2013) 1181–1187, http://dx.doi.org/10.2166/ws.2013.125.
[38] D. Setyono, S. Valiyaveettil, Functionalized paper-A readily accessible adsorbent for removal of dissolved heavy metal salts and nanoparticles from water, J. Hazard. Mater. 302 (2016) 120–128, http://dx.doi.org/10.1016/j.jhazmat.2015.09.046.
[39] K. Żelechowska, I. Kondratowicz, M. Gazda, Graphene hydrogels with embedded metal nanoparticles as efficient catalysts in 4-nitrophenol reduction and methylene blue decolorization, Pol. J. Chem. Technol. 18 (4) (2017) 47–55, http://dx.doi.org/10.1515/pjct-2016-0070.
[40] N.N. Long, L.V. Vu, C.H. Kiem, S.C. Doanh, C.T. Nguyet, P.T. Hang, N.D. Thien, L.M. Quynh, Synthesis and optical properties of colloidal gold nanoparticles, J. Phys.: Conf. Ser. 187 (2009) 012026, http://dx.doi.org/10.1088/1742-6596/187/1/012026.
[41] G. Luo, H. Huang, C. Lei, Z. Cheng, X. Wu, S. Tang, Y. Du, Facile synthesis of porous graphene as binder-free electrode for supercapacitor application, Appl. Surf. Sci 366 (2016) 46–52, http://dx.doi.org/10.1016/j.apsusc.2016.01.015.
[42] Z. Fan, Y. Tng, C.X. Ting Lima, P. Liu, S.T. Nguyen, P. Xiao, A. Marconnet, C.Y.H. Lima, H.M. Duong, Thermal and electrical properties of graphene/carbon nanotube aerogels, Colloids Surf. A 445 (2014) 48–53, http://dx.doi.org/10.1016/j.colsurfa.2013.12.083.
[43] Z. Sui, X. Zhang, Y. Lei, Y. Luo, Easy and green synthesis of reduced graphite oxide-based Hydrogels, Carbon 49 (2011) 4314–4321, http://dx.doi.org/10.1016/j.carbon.2011.06.006.
[44] J. Zhang, H. Yang, G. Shen, P. Cheng, J. Zhang, S. Guo, Reduction of graphene oxide via L-ascorbic acid, Chem. Commun. 46 (2010) 1112–1114, http://dx.doi.org/10.1039/B917705A.
[45] A.P. Goldstein, W. Mickelson, A. Machness, G. Lee, M.A. Worsley, L. Woo, A. Zettl, Simultaneous sheet cross-linking and deoxygenation in the graphene oxide sol-gel transition, J. Phys. Chem. C 118 (2014) 28855–28860, http://dx.doi.org/10.1021/jp5092027.
[46] H. Bai, C. Li, X. Wang, G. Shi, On the gelation of graphene oxide, J. Phys. Chem. C 115 (2011) 5545–5551, http://dx.doi.org/10.1021/jp1120299.
[47] J.W. Yoo, D.S. Yun, H.J. Kim, Influence of reaction parameters on size and shape of silica nanoparticles, J. Nanosci. Nanotechnol. 6 (11) (2006) 3343–3346, http://dx.doi.org/10.1166/jnn.2006.006.
[48] G.A. Rance, A.N. Khlobystov, Interactions of carbon nanotubes and gold nanoparticles: the effects of solvent dielectric constant and temperature on controlled assembly of superstructures, Dalton Trans. 43 (2014) 7400, http://dx.doi.org/10.1039/c3dt53372g.
[49] F. Wang, J. Zhao, M. Zhu, J. Yu, Y.-S. Hub, H. Liu, Selective adsorption–deposition of gold nanoparticles onto monodispersed hydrothermal carbon spherules: a reduction–deposition coupled mechanism, J. Mater. Chem. A 3 (2015) 1666, http://dx.doi.org/10.1039/C4TA05597G.